Angewandte Chemie International Edition

Angewandte International Edition Chemie

GDCh German Chemical Society

How to cite: *Angew. Chem. Int. Ed.* **2026**, e7643898
doi.org/10.1002/anie.7643898

RESEARCH ARTICLE

High-Purity Monovalent Functionalization of Carbon Nanotubes

Shoichi Nishitani[1] | Zirun Liang[1] | Ayana Tabo[2] | Wanlin Zhang[1] | Deverin Smith[1] | Ke Xu[2] | Markita P. Landry[3,4,5]

[1]Department of Chemical and Biomolecular Engineering, University of California, Berkeley, California, USA | [2]Department of Chemistry, University of California, Berkeley, California, USA | [3]Innovative Genomics Institute (IGI), Berkeley, California, USA | [4]California Institute for Quantitative Biosciences, QB3, University of California, Berkeley, California, USA | [5]Chan-Zuckerberg Biohub, San Francisco, California, USA

Correspondence: Shoichi Nishitani (snishitani@berkeley.edu)

Received: 21 February 2026 | **Revised:** 21 February 2026 | **Accepted:** 6 April 2026

Keywords: nanotechnology | near-infrared fluorescence | single-molecule | single-walled carbon nanotubes | TIRF

ABSTRACT

Single-walled carbon nanotubes (SWCNTs) show promise for probing molecular interactions at single-molecule resolution, yet generating SWCNT populations bearing a single defined functional tag remains challenging because surface functionalization is inherently stochastic. Here, we present a batch-scale strategy to produce predominantly singly tagged SWCNTs by leveraging the stochastic adsorption of single-stranded DNA (ssDNA). Specifically, SWCNTs are dispersed using a mixture of unmodified ssDNA (um-ssDNA) and a minor fraction of modified ssDNA (m-ssDNA) carrying an affinity handle. We developed a probabilistic ssDNA–SWCNT binding model that predicts the distribution of m-ssDNA per nanotube as a function of the input minor-strand fraction p = m-ssDNA/total ssDNA, enabling selection of conditions that maximize single-tag purity. Using magnetic-bead capture via a biotin affinity interaction and subsequent release, we isolate SWCNTs with 97.6% predicted single-tag purity at 2% recovery. Single-molecule fluorescence imaging further supports predominantly single-label occupancy under the model-selected conditions. Thus, this approach provides a general route to SWCNTs bearing a single molecular handle for downstream conjugation and assembly, supporting diverse future applications in SWCNT-based nanotechnologies.

1 | Introduction

Single-walled carbon nanotubes (SWCNTs) provide a unique one-dimensional platform for molecular transduction, combining nanoscale dimensions with highly sensitive electronic conductance and near-infrared (NIR) fluorescence [1, 2]. In single-molecule field-effect transistor (smFET) architectures, an individual nanotube is functionalized with a *single* biomolecule, enabling stochastic molecular events of that tethered molecule (e.g., turnover steps, binding/unbinding, or conformational transitions) to be resolved in real time as discrete conductance changes. For example, tethering a single enzyme to a SWCNT enables real-time electrical recordings of enzymatic processivity at the single-molecule level [3–5]. Likewise, single-aptamer–SWCNT smFETs can resolve aptamer–ligand binding kinetics through step-like conductance transitions [6]. Beyond bioelectronics, sparse covalent "quantum defects" in SWCNTs create bright, spectrally distinct emissive sites [7–9] and can exhibit room-temperature single-photon emission [10–12]—capabilities that critically depend on controlling defect number and distribution per nanotube [13, 14]. Likewise, deterministic nanoscale assembly (e.g., placement on DNA-origami scaffolds) benefits from a single addressable molecular handle per nanotube to avoid uncontrolled multi-point attachment and to program position and orientation [15, 16]. Collectively, these examples highlight a recurring need for dispersed SWCNT populations bearing

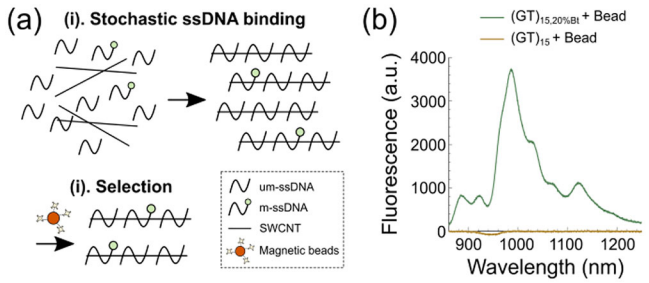

FIGURE 1 | Strategy for monovalent SWCNT functionalization and selective capture. (a) Schematic representation of the two-step process to achieve monovalent (singly tagged) SWCNTs: (i) stochastic adsorption of an ssDNA mixture containing a minor fraction of modified strands (m-ssDNA), and (ii) selective extraction of functionalized nanotubes via magnetic bead-assisted separation. (b) Proof-of-principle validation of capture selectivity: Representative NIR fluorescence spectra of streptavidin-coated magnetic beads after incubation with 20% Bt-$(GT)_{15}$–SWCNTs (green) and unmodified $(GT)_{15}$–SWCNTs (orange). The absence of a detectable NIR signal from the unmodified control confirms minimal nonspecific adsorption of the DNA–SWCNT complexes to the bead surface.

a defined, single molecular tag (or single reactive site) per nanotube; however, batch-scale routes to such "monovalent" SWCNTs remain limited.

Precisely controlling the valency of functional tags on SWCNTs remains challenging because surface functionalization is inherently stochastic across heterogeneous nanotube populations. Existing routes, therefore, often rely on low-conversion reactions [5, 17, 18]—frequently on surface-immobilized SWCNTs—followed by post hoc identification/selection of sparsely functionalized nanotubes using single-particle techniques such as atomic force microscopy (AFM) [3, 4]. For water-dispersed SWCNTs in solution, prior work has predominantly achieved end-selective (terminus-biased) conjugation, which restricts functionalization to the nanotube ends but does not generally provide population-level control of strict monovalency. In particular, oxidative end-functionalization produces a distribution of reactive groups, making it challenging to guarantee one-to-one coupling across a bulk sample [19, 20]. Consequently, batch-scale routes that yield dispersed SWCNT populations bearing a defined single reactive handle per nanotube remain limited. Here, we leverage ssDNA wrapping [21] and an affinity purification strategy to enrich high-purity, singly tagged SWCNTs in aqueous dispersion at a batch scale.

2 | Results and Discussion

Our strategy for achieving monovalent modification of SWCNTs involves a two-step process. First, we model a dispersion of SWCNTs in a pool of ssDNA, assuming that all ssDNA molecules have equal binding affinity to SWCNTs (Figure 1a). We incorporate a small quantity of modified ssDNA (m-ssDNA) into this mixture, which is either preconjugated with a biomolecule or chemically modified to allow postconjugation. This process yields individually dispersed ssDNA–SWCNTs, predominantly consisting of unmodified ssDNA (um-ssDNA) with a minor fraction of m-ssDNA. By gradually decreasing the m-ssDNA:um-ssDNA ratio, we anticipate reaching a point where most SWCNTs bearing m-ssDNA will contain only a single m-ssDNA molecule. Consequently, selective extraction of these SWCNTs containing m-ssDNA (m-ssDNA–SWCNTs) from the mixed dispersion results in a purified population of SWCNTs, each bearing a single tag (a single m-ssDNA strand), achieving monovalent (singly tagged) SWCNTs.

To selectively isolate m-ssDNA-tagged SWCNTs, we employ a magnetic bead-assisted separation strategy harnessing robust biotin (Bt)–streptavidin binding (Figure 1a) [22, 23]. We hypothesized that the exceptional binding affinity between biotin and streptavidin would facilitate the specific capture of small quantities of functionalized SWCNTs, with a possibility of nonspecific ssDNA-SWCNT adsorption to the magnetic beads. To quantify the degree of nonspecific adsorption to the beads, we used a biotin-labeled m-ssDNA sequence to disperse SWCNTs. Subsequently, we incubated the SWCNT dispersion with streptavidin-coated magnetic beads to capture and isolate m-ssDNA–SWCNTs from the ssDNA–SWCNTs population using magnets. Our results revealed effective capture of 20% Bt-$(GT)_{15}$–SWCNT, prepared as a 1:4 w/w mixture of biotinylated $(GT)_{15}$ and unmodified $(GT)_{15}$, as confirmed by SWCNT NIR fluorescence (Figure 1b). Notably, the absence of detectable signals from the $(GT)_{15}$–SWCNT control suggests that the capture process is primarily driven by biotin–streptavidin interactions, with minimal nonspecific adsorption to a level undetectable by NIR spectroscopy.

Motivated by the feasibility of our strategy to isolate small fractions of biotinylated SWCNTs from a larger population of unmodified SWCNTs, we conducted theoretical calculations to predict the quantitative distribution of m-ssDNA on SWCNTs as a function of m-ssDNA:um-ssDNA ratio in the starting mixture, considering $(GT)_{15}$ as a model ssDNA sequence. Adsorption of ssDNA on SWCNTs is a complex process that currently lacks comprehensive thermodynamic models, posing a challenge for predicting the final equilibrium state and, consequently, making reliable predictions [24, 25]. Therefore, to simplify the problem, we modeled ssDNA adsorption on SWCNTs as a stochastic process, assuming that um-ssDNA and m-ssDNA have comparable probabilities of occupying vacant binding sites. We expect this approximation to be most appropriate for sufficiently long ssDNA sequences, such as $(GT)_{15}$, and when the terminal modification does not substantially perturb ssDNA–SWCNT adsorption. This assumption was justified by a kinetic analysis of competitive binding, where a linear relationship between the input mixing ratio p and the surface occupancy confirms that both strands possess effectively identical adsorption rate constants (Figure S1). Our experimental data exhibited a strong linear correlation ($R^2 > 0.99$) with a slope of 0.8, which is in close agreement with the ideal stochastic limit (slope = 1.0; see Figure S1 and Supporting Information for the full kinetic derivation). Under these conditions, the model reduces to sampling SWCNT-binding strands from the original ssDNA pool, governed primarily by the relative abundance of m-ssDNA versus um-ssDNA.

We note that bulky cargos appended to ssDNA may reduce adsorption through steric effects, whereas highly π-conjugated moieties could enhance adsorption via additional π–π interactions. In such cases, unequal adsorption propensities can be

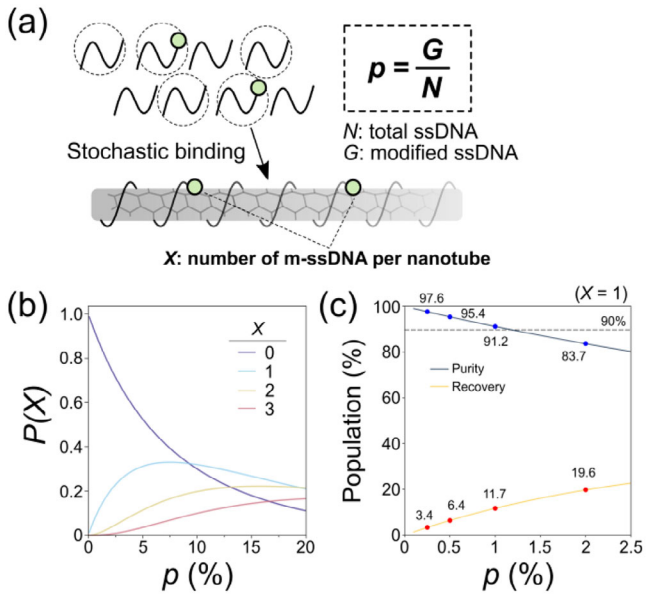

FIGURE 2 | Theoretical estimation of the probability of m-ssDNA:um-ssDNA ratio-dependent m-ssDNA population on SWCNTs. (a) Schematic representation of probability distribution as a random selection of SWCNT-binding ssDNA from the entire ssDNA pool, assuming equal binding probability for all ssDNA molecules. (b) Binomial probability distributions of finding specific m-ssDNA counts of $X = 0$ (purple), 1 (blue), 2 (yellow), and 3 (pink) as a function of p. (c) Percent purity of the recovered ($X \geq 1$) population (blue) and theoretical maximum recovery of singly modified SWCNTs, $100 \times P(X = 1)$ (yellow) as a function of p, with points specifically shown at $p =$ 0.25%, 0.5%, 1%, and 2%. The dashed line indicates 90% purity of singly modified SWCNTs. Details of these statistical metrics are explained in the Supporting Information.

captured by introducing a relative binding-weight parameter for m-ssDNA versus um-ssDNA. Because this parameter depends on the appended cargo and experimental conditions, it must be determined empirically and is beyond the scope of this work. Alternatively, bulky cargos (e.g., proteins) can be introduced via postconjugation by first purifying SWCNTs bearing a single orthogonal chemical handle.

To derive the probability model, we considered a simplified scenario in which a single SWCNT with a specific dimension is placed in a pool of ssDNA (Figure 2a). Subsequently, the probability distribution is conceptualized as a process of random ssDNA selection binding to the SWCNT, with the variable X representing the number of m-ssDNA molecules within the selected population. Assuming that ssDNA binding occurs without replacement, X can be described by a hypergeometric distribution:

$$X \sim Hypergeometric(N, G, n) \tag{1}$$

where N denotes the total number of ssDNA molecules in the pool, G the total number of m-ssDNA molecules, and n the number of ssDNA bound to the SWCNT at saturation, equivalent to the surface coverage. This model is physically justified by the irreversible nature of ssDNA adsorption [26]; once a strand wraps around a nanotube, it is effectively removed from the available pool on experimental timescales, mapping the binding process directly to sampling without replacement (see the Methods section in the Supporting Information). Thus, the exact probability for a specific value of $X = k$ is expressed as:

$$P\ (X = k) = \frac{\binom{G}{k}\binom{N-G}{n-k}}{\binom{N}{n}} \tag{2}$$

While N is on the order of 10^{15} in our experimental conditions, rendering computation impractical, X can be approximated by a binomial distribution under the condition $N >> n$. Intuitively, the hypergeometric distribution describes sampling n strands from a finite pool without replacement; when $N >> n$, this becomes effectively equivalent to independent sampling with probability p, yielding a binomial distribution. Here, $p = G/N$ is the fraction of m-ssDNA in the starting ssDNA pool. For $(GT)_{15}$-SWCNT complexes, we determined the average SWCNT length to be 301 nm by AFM (Figure S2), and estimated an ssDNA number density ($d = n/L$) of 0.05 nm^{-1} by fluorescence quantification of displaced $(GT)_{15}$-FAM (Figure S3) combined with the length-dependent theoretical SWCNT molecular weight (Figure S4). Consequently, X and its corresponding probability for $X = k$ can be expressed as:

$$X \sim Binomial\,(n,\ p) \tag{3}$$

$$P\,(X = k) = \binom{n}{k} p^k (1-p)^{n-k} \tag{4}$$

Where $p = G/N$, representing the m-ssDNA:um-ssDNA ratio. Thus, the probability of m-ssDNA on SWCNT at $X = k$, given a specific surface coverage n, is solely a function of p. Finally, to generalize this equation, we incorporated SWCNT length variation as a conditional probability. Here, we determined surface coverage, n, as a function of SWCNT length by assuming a linear relationship between surface coverage and SWCNT length (see Methods section in the Supporting Information for details). Thus, the final expression of $P(X = k)$ is:

$$P\,(X = k) = \sum_{\forall n} P(X = k|n_i)P\,(n_i) = \sum_{\forall n} \binom{n_i}{k} p^k (1-p)^{n_i - k} P\,(n_i) \tag{5}$$

Where n_i is the surface coverage of SWCNT with length l, and $P(n_i)$ is the probability of finding SWCNT with length l.

Figure 2b depicts the binomial probabilities of finding specific m-ssDNA counts ($X = 0$, 1, 2, and 3) on a SWCNT as a function of p. Accordingly, the probability of achieving a single m-ssDNA on SWCNT, $P(X = 1)$, reaches its maximum value of 0.331 at a 7.5% mixture of m-$(GT)_{15}$ in the ssDNA pool ($p = 7.5\%$). However, at this m-ssDNA ratio, we anticipate a considerable population of SWCNTs with 2 and 3 m-ssDNA molecules. Figure S5 compares the probability distributions of finding specific m-ssDNA counts (0, 1, 2, 3, 4, and 5) at low m-ssDNA ratios (0.25%, 0.5%, 1.0%, 2.0%, and 4.0%). At 1% m-ssDNA, probabilities for $X > 2$ become negligibly small, with combined probabilities of $X = 0$, 1, and 2 summing to 0.999. Therefore, assuming a complete isolation of the SWCNT population holding m-ssDNA, 91.1% of SWCNTs will possess only a single m-ssDNA molecule (91.1% purity of singly modified SWCNTs). Furthermore, at $p = 0.5\%$, this percentage

reaches 95.4% with a corresponding predicted recovery yield of 6.4%. Figure 2c shows the relationship between purity and percent recovery as a function of p, highlighting the trade-off between the two. Here, we define the "percent recovery" as the theoretical fraction of all SWCNTs expected to carry exactly one m-ssDNA strand, i.e., $100 \times P(X = 1)$, representing the upper bound under ideal capture and release. Thus, this probability model enables the quantitative determination of the optimal m-ssDNA:ssDNA ratio for the target purity and yield of singly modified SWCNTs.

Our probability model indicates that achieving a single m-ssDNA modification in above 90% of the recovered SWCNT population requires an initial ssDNA pool containing less than 1% m-ssDNA. This scenario predicts a maximum yield of 11.7%, with the remaining 88.3% of SWCNTs absent from m-ssDNA. Such a limited yield requires an experimental separation process sensitive enough to isolate sufficient quantities of functionalized SWCNTs. Thus, as a next step, we evaluated the efficacy of magnetic bead-assisted separation strategies for selectively isolating functionalized SWCNTs dispersed at m-ssDNA concentrations below 1%, targeting a recovered population in which the dominant species carries exactly one m-ssDNA strand. To recover captured SWCNTs from the beads, we incorporated a photocleavable (pc) spacer between m-ssDNA and biotin (Figure 3a) [27]. The detailed structure and mechanism of cleavage are illustrated in Figure S6. In this study, we employed $(GT)_{15}$ as the representative ssDNA sequence based on its demonstrated ability to effectively disperse SWCNTs and maintain colloidal stability of the resulting complexes [28].

Thus, our m-ssDNA design incorporated a biotin conjugation at the 5'-end of $(GT)_{15}$ via pc linker to facilitate separation of functionalized SWCNTs. Concurrently, carboxyfluorescein (FAM) was conjugated to the 3'-end of the sequence, serving both as a model of molecular functionalization and as a means to validate monovalent modification. We prepared ssDNA–SWCNT complexes using a standard tip-based sonication method. Our general separation procedure for functionalized SWCNTs involved mixing 2.5 μg of ssDNA–SWCNT with streptavidin-coated magnetic beads in phosphate-buffered saline (PBS) supplemented with 0.1% BSA to mitigate nonspecific adsorption. After incubation, captured m-ssDNA–SWCNTs were isolated from the unbound counterparts by multiple rounds of washing. Finally, captured SWCNTs were recovered by irradiation with 362 nm UV light for 1 h. The recovered SWCNTs were quantified by NIR fluorescence spectroscopy by measuring the fluorescence spectra of supernatant-recovered SWCNTs versus the fluorescence spectra of SWCNTs still attached to the magnetic beads.

Figure 3b illustrates the representative NIR fluorescence spectra of 0.25% pcBt$(GT)_{15}$FAM–SWCNT [pcBt$(GT)_{15}$FAM:$(GT)_{15}$ = 1:399, or p = 0.25%] following magnetic bead-assisted separation. Accordingly, even for the lowest m-ssDNA ratio of 0.25%, theoretically achieving 97.6% purity of singly modified SWCNTs (Figure 2c), the separation process yielded an appreciable amount of SWCNTs (Figure 3b, green). Notably, comparison of the (6,5) chirality peak between recovered SWCNTs (green) and SWCNTs retained on the beads (yellow) indicates a recovery efficiency of 88% (after correcting for a minor bead-induced optical enhancement; see Figure S7 and Supporting Information for details), highlighting the effectiveness of the inclusion of a photocleavable linker. We quantified SWCNT recoveries using the (6,5) chirality peak and found that 0.05 μg of SWCNT was recovered from the total 2.5 μg, corresponding to 2% recovery. As our probability model predicts a 0.25% m-ssDNA ratio to yield a SWCNT population with m-ssDNA of 3.4%, the experimental recovery efficiency of 2% is in close agreement with the prediction, validating both the probability model and the effectiveness of our recovery strategy. Notably, the negative control using $(GT)_{15}$–SWCNT ($p = 0$) yielded both negligible capture and recovery of SWCNTs, demonstrating high selectivity of the separation process (Figure 3c).

Desthiobiotin (dtBt) provides an alternative recovery route when UV irradiation is incompatible. dtBt is a biotin analog that binds streptavidin but with a weaker, reversible affinity, enabling recovery via competitive affinity exchange with free biotin (Figure 3d and Figure S8) [29]. dtBt-tagged SWCNTs were captured on streptavidin magnetic beads following the same procedure as pcBt. Captured SWCNTs were then released by incubation with 0.01 mg/mL biotin in PBS for 30 min, and the process was repeated three times. We recovered 44%, 25%, and 15% of the functionalized SWCNTs in the first, second, and third rounds, respectively (Figure S9), corresponding to a total recovery efficiency of 84% (Figure 3e), with negligible capture and recovery from the non-biotinylated control (Figure 3f). These results demonstrate that biotin–streptavidin interactions enable sensitive isolation of small quantities of functionalized SWCNTs and provide a UV-free recovery option well suited for downstream handling. Notably, the two linkers offer complementary advantages: pcBt yields SWCNTs recovered without a residual affinity handle after photocleavage (Figure S6), whereas dtBt recovery retains the dtBt functionality on the ssDNA (Figure S8), which can be advantageous for downstream workflows that directly leverage this affinity handle (e.g., surface immobilization or subsequent affinity-mediated conjugation), as used in our later experiments.

To experimentally assess whether the bulk labeling data are consistent with predominantly monovalent SWCNTs, we designed a fluorescence-based experiment utilizing the same m-ssDNA sequence, pcBt$(GT)_{15}$FAM. FAM is one of the most commonly used fluorophores that exhibit stable fluorescence with excitation/emission peaks at 495/520 nm. As our separation process includes UV exposure at 362 nm, it is important to choose a fluorophore whose absorbance does not overlap with this wavelength range. To confirm spectral separation, we conducted control experiments to assess the potential impact of UV irradiation on fluorophore stability. We confirmed that exposure to 362 nm UV light for 1 h does not induce detectable photobleaching of FAM (Figure S10), thereby ensuring that the quantified fluorescence signals accurately reflect the amount of recovered m-ssDNA without confounding artifacts from dye degradation.

SWCNTs are known to effectively quench organic dyes, a property that has been extensively exploited to probe the ssDNA-SWCNT surface corona [30–33]. Because FAM emission is strongly quenched while the labeled ssDNA is adsorbed on the SWCNT surface, we quantify the number of FAM-labeled strands by fully displacing ssDNA into solution by heating with sodium deoxycholate (SDC), where fluorescence is recovered and scales with the amount of released ssDNA–FAM. After normalizing SWCNT concentration by NIR emission, the recovered FAM

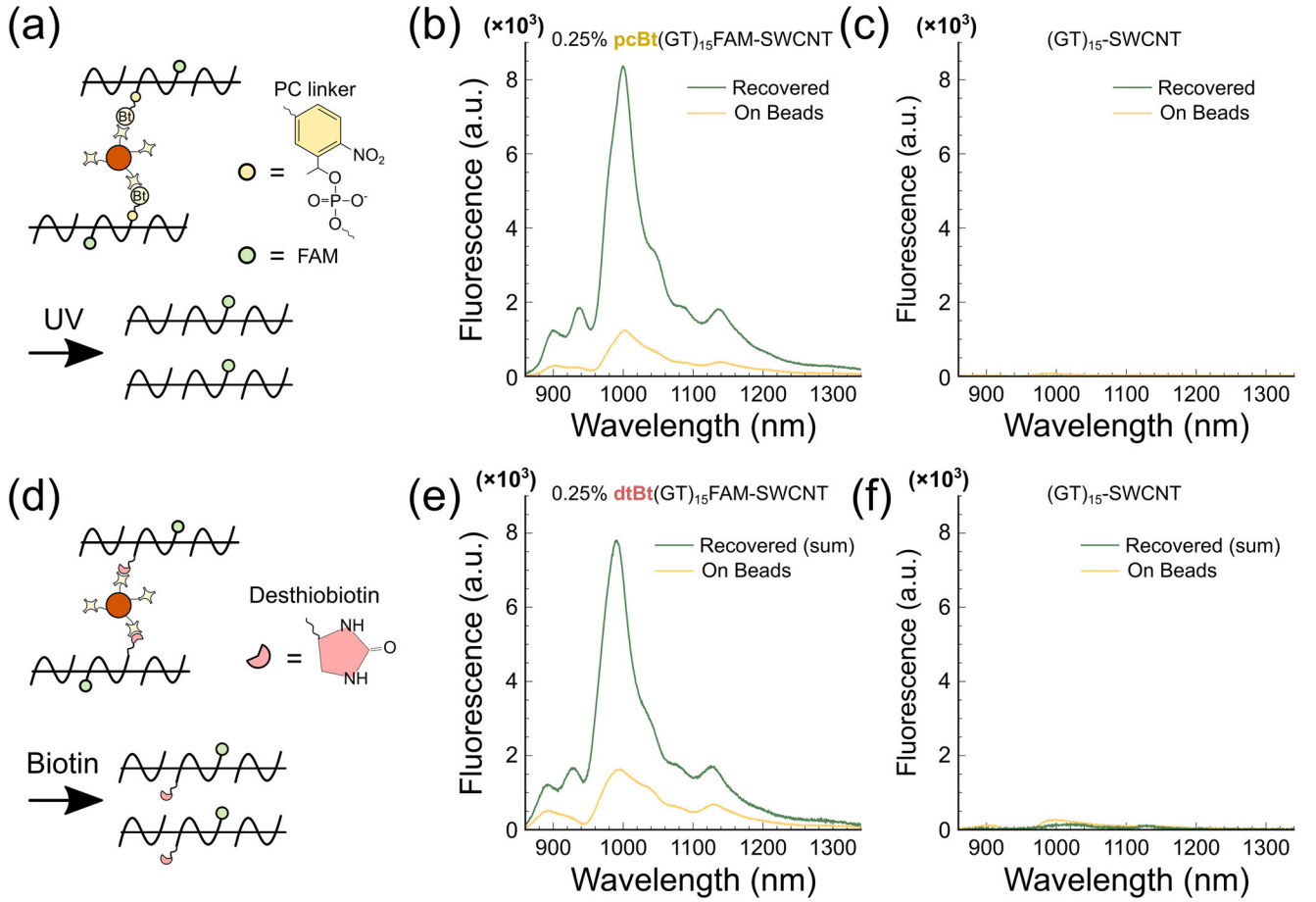

FIGURE 3 | Magnetic bead-assisted selective recovery of biotinylated ssDNA–SWCNTs via biotin–streptavidin interactions. (a) Conceptual illustration of selective recovery using a photo-cleavable biotin (pcBt) linker. (b, c) Representative NIR fluorescence spectra of 0.25% pcBt$(GT)_{15}$FAM–SWCNT (b) and $(GT)_{15}$–SWCNT control (c) after bead capture (yellow) and after UV-triggered recovery (green). (d) Conceptual illustration of UV-free recovery using desthiobiotin (dtBt) through competitive affinity exchange with free biotin. (e, f) Representative cumulative NIR fluorescence spectra of 0.25% dtBt$(GT)_{15}$–SWCNT (e) and $(GT)_{15}$–SWCNT control (f) after three recovery rounds. Same color schemes as (b, c) are used.

signal provides a direct readout of the average number of FAM-labeled strands per SWCNT across different values of p. Since our recovered functionalized SWCNTs contain at least one m-ssDNA, we hypothesize that as we decrease the fraction of m-ssDNA in the mixture, we would observe saturation of FAM fluorescence at a minimum value that remains significantly above background levels. Within our probabilistic framework, such saturation is expected when the recovered population is dominated by SWCNTs carrying a single FAM-labeled strand. To test this hypothesis as a bulk-level consistency check of the model, we selected five different m-ssDNA ratios based on our probability predictions: 0.25%, 0.5%, 1%, 2%, and 4%. After purifying functionalized SWCNTs by the previously described magnetic bead-based procedure, we normalized the SWCNT concentration by NIR fluorescence intensity at the (6,5) chirality peak. Subsequently, we employed a surfactant-based surface-exchange method to completely displace ssDNA from the SWCNTs, followed by quantitative fluorescence measurements.

Figure 4 illustrates the comparative analysis of FAM fluorescence intensities across the range of m-ssDNA ratios examined. We observed a statistically significant, consistent decrease in FAM fluorescence intensity correlating with a reduction in the m-ssDNA ratio from 4% to 1%. Of particular significance, our statistical analysis revealed that FAM fluorescence reaches a saturating value at 1% m-ssDNA, showing no statistically significant difference between 1%, 0.5%, and 0.25%. This result aligns with our probability model's prediction that, at 1% m-ssDNA, the population of recovered SWCNTs containing at least one m-ssDNA is predominantly singly modified. Thus, our probability-based conceptualization of ssDNA adsorption on SWCNTs successfully predicts the observed bulk FAM fluorescence behavior across m-ssDNA ratios. Furthermore, the statistically significant difference between the blank and the saturated fluorescence level indicates successful recovery of singly modified SWCNTs, but with the caveat that the bulk FAM assay, by itself does not resolve the population-level exact copy number per individual nanotube.

Since the FAM–SWCNT relationship can be treated as equimolar at saturation, we estimate the SWCNT molar concentration to be $\sim 3.8 \times 10^{-10}$ mol/L. We note that this value should be interpreted as an effective estimate, as calibration at low fluorescence levels introduces uncertainty. Nevertheless, as the mass and dimensional variability of SWCNT samples make exact quantification challenging, our methodology developed herein may contribute to the fundamental characterization of SWCNT conjugates.

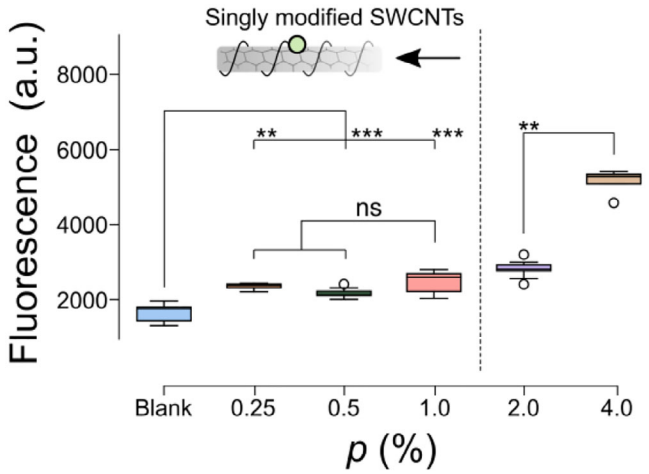

FIGURE 4 | Validation of single-FAM modification on SWCNTs by bulk fluorescence quantification. FAM fluorescence intensity is plotted as a function of the minor-strand fraction p (%) = m-ssDNA/total ssDNA. SWCNT concentrations for all samples were first normalized by NIR fluorescence before FAM quantification. Data points represent independent separation experiments (N), each averaged over 16 microwell regions. Statistical differences between FAM intensity distributions at different values of p were assessed using a two-sample Kolmogorov-Smirnov test (two-sided). Significance levels are indicated as $^{***}p < 0.001$, $^{**}0.001 < p < 0.01$, and $^{*}0.01 < p < 0.05$; ns denotes $p > 0.05$. These results support predominantly single-FAM modification of SWCNTs at $p = 1\%$.

We next sought to verify single-tag occupancy at the level of individual SWCNTs using single-molecule total internal reflection fluorescence (smTIRF) microscopy, because our experiments in Figure 4 rely on bulk fluorescence readouts that do not reflect population distributions at the single-SWCNT level. For these measurements, we prepared 1% and 15% m-ssDNA samples using the exact stoichiometry as in the other experiments, but replacing the minor component with $(GT)_{15}T_{20}$, with dtBt and Cy5 tags at the 5' and 3' ends, respectively. Here, dtBt serves a dual role: it enables affinity exchange and recovery from magnetic beads, and it provides a handle for immobilizing these SWCNTs onto biotin–PEG-coated glass surfaces via neutravidin for smTIRF imaging (Figure 5a). The additional T_{20} tail is incorporated to mitigate Cy5 quenching by the SWCNT surface; by hybridizing a complementary A_{20} strand, the Cy5 label is positioned on a short double-stranded DNA spacer that lifts the fluorophore away from the nanotube [34]. Note that additional measurements indicate that the number of ssDNA strands adsorbed per SWCNT is essentially unchanged between $(GT)_{15}$ and $(GT)_{15}T_{20}$ (Figure S11). Because the T_{20} segment likely does not adsorb on the SWCNT and remains flexible in solution, this modification is not expected to perturb the ssDNA adsorption statistics that underlie our model [35].

smTIRF imaging provides access to single-fluorophore photobleaching trajectories for Cy5–SWCNT complexes and thus directly reports on the Cy5 copy number per nanotube. We immobilized Cy5-labeled SWCNTs prepared with 1% or 15% Cy5-labeled ssDNA in the ssDNA mixture and recorded fluorescence movies under identical excitation power and acquisition settings (Figure S12). Individual diffraction-limited spots were localized, and their intensity time traces were analyzed using the hidden Markov model (HMM)-based step-finding procedure. For each trace, we extracted the fluorescence intensity change ΔI of the prebleach "on" state relative to the post-bleach baseline (i.e., $\Delta I = I_{on} - I_{baseline}$), and, independently, the number of discrete bleaching steps n_{steps} assigned by the HMM (Figure 5b,c). Because all measurements were acquired at the same excitation intensity and optical configuration, we expect ΔI to increase approximately with the number of Cy5 molecules per SWCNT; thus, the ΔI distribution provides an intensity-based check that is conceptually orthogonal to the step-counting analysis.

The ΔI histograms (Figure 5b) and step-number histograms (Figure 5c) analyzed from smTIRF imaging together show consistent results with the predicted number of m-ssDNAs and experimental results of the bulk fluorescence measurement. For the 1% sample, the ΔI distribution is narrowly peaked at lower amplitudes, whereas the 15% sample exhibits a broader distribution extending to higher intensities, indicating that Cy5–SWCNT spots in the 15% condition, on average, emit more photons before bleaching. Separately, the HMM-based step analysis reveals that the vast majority of traces in the 1% sample display a single bleaching step ($n_{steps} = 1$), whereas the 15% sample shows a substantial population of multi-step traces ($n_{steps} > 2$). Thus, the intensity-based ΔI shift and the independently obtained step-number distribution are mutually consistent: the condition that produces more multistep traces also produces higher prebleach intensities. Quantitatively, approximately 90% of traces in the 1% condition are classified as single-step events, in good agreement with the purity expected from our statistical model for 1% m-ssDNA loading. Thus, together with the bulk fluorescence results, we have successfully achieved predominantly monovalent fluorophore modification on SWCNTs.

3 | Conclusion

In this study, we developed a DNA-guided, facile methodology to generate and purify monovalent (singly tagged) SWCNTs at scales beyond those achievable with existing methods. First, we dispersed SWCNT with single-stranded DNA (ssDNA) mixed with a small fraction of functionalized ssDNA (m-ssDNA). We developed a stochastic ssDNA–SWCNT binding model to determine a m-ssDNA-ratio-dependent quantitative distribution of m-ssDNA on SWCNTs. The binomial distribution model predicted that, at an m-ssDNA ratio of 1%, 91.2% of isolated SWCNTs carrying at least one m-ssDNA would bear exactly one m-ssDNA tag (monovalent purity of 91.2%). We then implemented magnetic bead-based separation to selectively isolate singly modified SWCNTs from unmodified SWCNTs, using $(GT)_{15}$ and $(GT)_{15}$-FAM as model ssDNA sequences. Consequently, we recovered functionalized SWCNTs with 2% yield and 80% efficiency at an m-ssDNA ratio as low as 0.25%, corresponding to a model-predicted purity of 97.6% singly modified SWCNTs.

Bulk FAM fluorescence quantification as a function of m-ssDNA fraction showed saturation of FAM signal at and below 1%, consistent with this probabilistic model when combined with the constraint that all recovered SWCNTs carry at least one FAM-labeled strand. Finally, we directly validated single-tag occupancy using single-molecule TIRF (smTIRF) microscopy, in which photobleaching-step analysis revealed that at 1% m-ssDNA, the

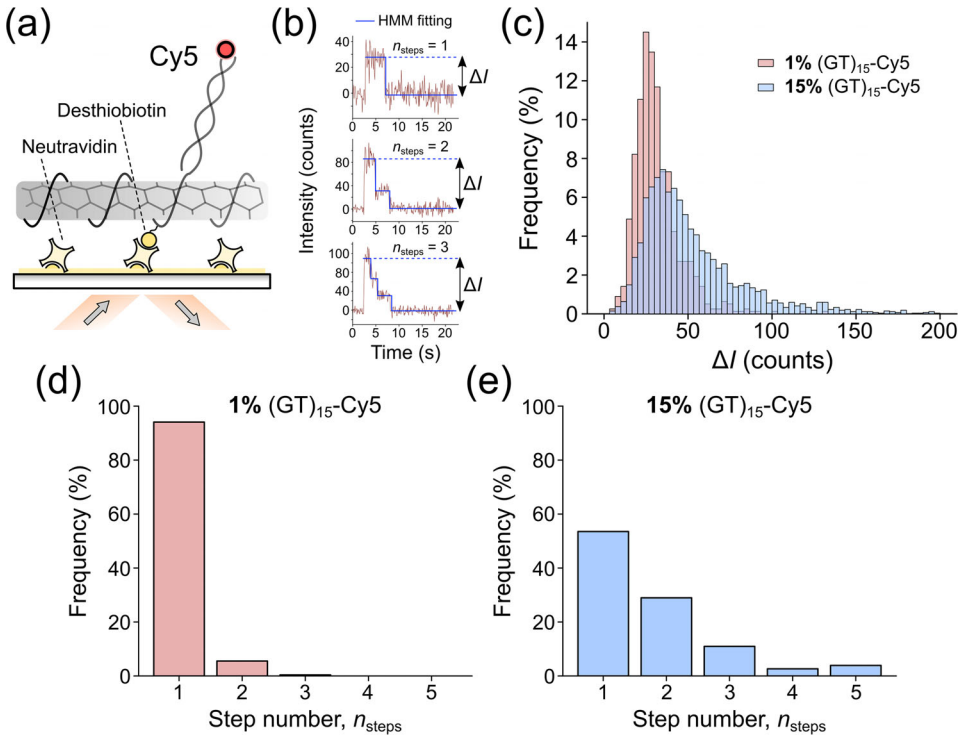

FIGURE 5 | Verification of single-fluorophore modification by smTIRF-based photobleaching-step quantification. (a) Schematic of ssDNA-SWCNTs immobilized on a coverslip and imaged by smTIRF microscopy. Individual Cy5 fluorophores attached to ssDNA on a single SWCNT undergo discrete photobleaching events that report the number of Cy5 tags per nanotube (b) Representative traces (background subtracted) of one, two, and three discrete bleaching events. (c) Distribution of prebleach fluorescence intensity (ΔI) extracted from HMM fits to Cy5 intensity traces for SWCNTs prepared with 1% or 15% Cy5-tagged ssDNA in the mixture. Here, ΔI is defined as the intensity difference between the prebleach "on" state (turn-on plateau) and the postbleach baseline for each trace. (d, e) Histograms of the number of bleaching steps per spot, reporting the Cy5 copy number per SWCNT, for 1% (d) and 15% (e) conditions. Data in (c–e) are pooled from two independent preparations per condition, each imaged over 7 fields of view (14 FOV total).

vast majority of SWCNTs exhibit a single bleaching step and a corresponding narrow intensity distribution, whereas higher m-ssDNA fractions give multistep trajectories and higher intensities. Together, the model, bulk fluorescence measurements, and single-molecule imaging provide convergent evidence that our separation protocol yields SWCNT populations that are predominantly singly modified. Conventional approaches for monovalent SWCNT modification typically rely on minimizing reaction efficiency, resulting in low purity and recovery yield, or are restricted to surface-immobilized SWCNTs. Thus, the methodology described herein offers an alternative, facile route to high-purity, singly tagged SWCNTs in aqueous dispersion.

Although we have employed $(GT)_{15}$–SWCNT as a representative system, our methodology is intrinsically generalizable to a wide range of ssDNA–SWCNT combinations. The stochastic model is fundamentally governed by the ssDNA binding density (d), a parameter that can be readily determined experimentally for any specific sequence–nanotube pair. As demonstrated by our parametric study (Figure S13), the strategy remains robust across diverse packing densities. We evaluated a range of binding densities from 0.03 to 0.1 nm^{-1}, corresponding to the estimated surface footprints of $(GT)_n$ sequences with repeat numbers n ranging from 30 to 6, respectively. For systems with higher ssDNA binding densities, the initial mixing ratio p can be strategically adjusted to consistently yield monovalent nanotubes with high single-tag purity. Furthermore, while our model assumes equal adsorption propensities for m-ssDNA and um-ssDNA, it can be generalized to more complex modifications by incorporating a weighted sampling parameter for cargos that substantially perturb adsorption energy. This versatility positions our approach as a flexible platform for the precision engineering of functionalized carbon nanotubes.

We acknowledge that operating at low minor-strand fractions p to enrich singly tagged SWCNTs is inherently low-yielding, because most nanotubes carry no modified strand and therefore cannot be captured; accordingly, further process optimization will be important to increase throughput for specific applications, or recovery and recycling of unmodified SWCNT material can be implemented to decrease material loss.

Finally, a notable advantage of our strategy is its molecule-independent flexibility: the use of chemically modified ssDNA (m-ssDNA) enables purification of SWCNTs bearing a single orthogonal reactive handle, which can subsequently be used for post-conjugation of diverse cargos (including bulky biomolecules). We also envision applying this strategy to control SWCNT defects at the single-defect scale, thereby enabling improved design of imaging probes and other functional nanodevices including single-photon emitters. In conclusion, our approach provides a new batch-scale method for producing SWCNT samples predominantly tagged with a single molecular

label, supporting diverse future applications in SWCNT-based nanotechnologies.

Author Contributions

S.N. and Z.L. contributed equally to this work and reserve the right to prioritize their names on the author list when presenting or reporting on this work. S.N. conceived the project and designed the experiments. Z.L. developed the probability model and performed the calculations. S.N., Z.L., A.T., W.Z., and D.S. performed the experiments. S.N. and Z.L. analyzed the data, prepared the figures, and wrote the manuscript. M.P.L. and K.X. provided technical guidance and editorial input. All authors contributed to the discussion and assisted in the editing of the final manuscript.

Acknowledgements

We acknowledge support of a CZI Imaging Award, a Burroughs Wellcome Fund Career Award at the Scientific Interface (CASI) (to M.P.L.), a Dreyfus foundation award (to M.P.L.), a Schmidt Polymaths Award (to M.P.L), an NSF CBET award (to M.P.L.), a Sloan Foundation Award (to M.P.L.), a Moore Foundation Award (to M.P.L.), and a McKnight Scholar Award (to M.P.L.). M.P.L. is a Chan Zuckerberg Biohub investigator, a Helen Wills Neuroscience Institute Investigator, and an IGI Investigator. A.T. and K.X. were supported by STROBE, a National Science Foundation Science and Technology Center under Grant Number. DMR 1548924.

Conflicts of Interest

The authors declare no conflicts of interest.

Data Availability Statement

The data that support the findings of this study are available from the corresponding author upon reasonable request.

References

1. C. Gu, C. Jia, and X. Guo, "Single-Molecule Electrical Detection With Real-Time Label-Free Capability and Ultrasensitivity," *Small Methods* 1 (2017): 1700071, https://doi.org/10.1002/smtd.201700071.

2. H. Ju, L. Cheng, M. Li, et al., "Single-Molecule Electrical Profiling of Peptides and Proteins," *Advancement of Science* 11 (2024): e2401877, https://doi.org/10.1002/advs.202401877.

3. Y. Choi, I. S. Moody, P. C. Sims, et al., "Single-Molecule Lysozyme Dynamics Monitored by an Electronic Circuit," *Science* 335 (2012): 319–324, https://doi.org/10.1126/science.1214824.

4. T. J. Olsen, Y. Choi, P. C. Sims, et al., "Electronic Measurements of Single-Molecule Processing by DNA Polymerase I (Klenow Fragment)," *Journal of the American Chemical Society* 135 (2013): 7855–7860, https://doi.org/10.1021/ja311603r.

5. Y. Choi, T. J. Olsen, P. C. Sims, et al., "Dissecting Single-Molecule Signal Transduction in Carbon Nanotube Circuits With Protein Engineering," *Nano Letters* 13 (2013): 625–631, https://doi.org/10.1021/nl304209p.

6. Y. Lee, J. Buchheim, B. Hellenkamp, et al., "Carbon-nanotube Field-effect Transistors for Resolving Single-molecule Aptamer–ligand Binding Kinetics," *Nature Nanotechnology* 19 (2024): 660–667, https://doi.org/10.1038/s41565-023-01591-0.

7. Y. Piao, B. Meany, L. R. Powell, et al., "Brightening of Carbon Nanotube Photoluminescence Through the Incorporation of sp^3 Defects," *Nature Chemistry* 5 (2013): 840–845, https://doi.org/10.1038/nchem.1711.

8. Y. Miyauchi, M. Iwamura, S. Mouri, T. Kawazoe, M. Ohtsu, and K. Matsuda, "Brightening of Excitons in Carbon Nanotubes on Dimensionality Modification," *Nature Photonics* 7 (2013): 715–719, https://doi.org/10.1038/nphoton.2013.179.

9. F. L. Sebastian, N. F. Zorn, S. Settele, et al., "Absolute Quantification of sp 3 Defects in Semiconducting Single-Wall Carbon Nanotubes by Raman Spectroscopy," *Journal of Physical Chemistry Letters* 13 (2022): 3542–3548, https://doi.org/10.1021/acs.jpclett.2c00758.

10. D. Kozawa, Y. Shiota, M. Wang, and Y. K. Kato, "Deterministic Formation of Single Organic Color Centers in Single-Walled Carbon Nanotubes," *Nano Letters* 25 (2025): 13103–13109, https://doi.org/10.1021/acs.nanolett.5c02378.

11. X. He, N. F. Hartmann, X. Ma, et al., "Tunable Room-temperature Single-photon Emission at Telecom Wavelengths From sp^3 Defects in Carbon Nanotubes," *Nature Photonics* 11 (2017): 577–582, https://doi.org/10.1038/nphoton.2017.119.

12. X. He, H. Htoon, S. K. Doorn, et al., "Carbon Nanotubes as Emerging Quantum-light Sources," *Nature Materials* 17 (2018): 663–670, https://doi.org/10.1038/s41563-018-0109-2.

13. F. L. Sebastian, S. Settele, H. Li, B. S. Flavel, and J. Zaumseil, "How to Recognize Clustering of Luminescent Defects in Single-wall Carbon Nanotubes," *Nanoscale Horiz* 9 (2024): 2286–2294, https://doi.org/10.1039/D4NH00383G.

14. S. Settele, F. J. Berger, S. Lindenthal, et al., "Synthetic Control Over the Binding Configuration of Luminescent sp^3-defects in Single-walled Carbon Nanotubes," *Nature Communications* 12 (2021): 2119, https://doi.org/10.1038/s41467-021-22307-9.

15. H. T. Maune, S.-P. Han, R. D. Barish, et al., "Self-assembly of Carbon Nanotubes Into Two-dimensional Geometries Using DNA Origami Templates," *Nature Nanotechnology* 5 (2010): 61–66, https://doi.org/10.1038/nnano.2009.311.

16. A.-P. Eskelinen, A. Kuzyk, T. K. Kaltiaisenaho, et al., "Assembly of Single-Walled Carbon Nanotubes on DNA-origami Templates Through Streptavidin–Biotin Interaction," *Small* 7 (2011): 746–750.

17. H. Wilson, S. Ripp, L. Prisbrey, et al., "Electrical Monitoring of sp 3 Defect Formation in Individual Carbon Nanotubes," *J Phys Chem C Nanomater Interfaces* 120 (2016): 1971–1976, https://doi.org/10.1021/acs.jpcc.5b11272.

18. S. S. Jang, S. Dubnik, J. Hon, et al., "Characterizing the Conformational Free-Energy Landscape of RNA Stem-Loops Using Single-Molecule Field-Effect Transistors," *Journal of the American Chemical Society* 145 (2023): 402–412, https://doi.org/10.1021/jacs.2c10218.

19. M. Freeley, H. L. Worthy, R. Ahmed, et al., "Site-Specific One-to-One Click Coupling of Single Proteins to Individual Carbon Nanotubes: A Single-Molecule Approach," *Journal of the American Chemical Society* 139 (2017): 17834–17840, https://doi.org/10.1021/jacs.7b07362.

20. B. Liu, B. Demir, C. A. Gultakti, et al., "Self-Aligning Nanojunctions for Integrated Single-Molecule Circuits," *ACS Nano* 18 (2024): 4972–4980, https://doi.org/10.1021/acsnano.3c10844.

21. M. Zheng, A. Jagota, E. D. Semke, et al., "DNA-assisted Dispersion and Separation of Carbon Nanotubes," *Nature Materials* 2 (2003): 338–342, https://doi.org/10.1038/nmat877.

22. J. Jeong, Y.-J. Lee, Y. S. Hwang, and I. S. Hong, "Selective Detection and Quantification of Carbon Nanotubes in Soil," *Environmental Toxicology and Chemistry* 34 (2015): 1969–1974, https://doi.org/10.1002/etc.3035.

23. K. Kojima, Y. Iizumi, M. Zhang, and T. Okazaki, "Streptavidin-Conjugated Oxygen-Doped Single-Walled Carbon Nanotubes as Near-Infrared Labels for Immunoassays," *Langmuir* 38 (2022): 1509–1513, https://doi.org/10.1021/acs.langmuir.1c02824.

24. F. Albertorio, M. E. Hughes, J. A. Golovchenko, and D. Branton, "Base Dependent DNA–carbon Nanotube Interactions: Activation Enthalpies and Assembly–disassembly Control," *Nanotechnology* 20 (2009): 395101, https://doi.org/10.1088/0957-4484/20/39/395101.

25. S. Tonoyan, D. Khechoyan, Y. Mamasakhlisov, and A. Badasyan, "Statistical Mechanics of DNA-nanotube Adsorption," *Physical Review E* 101 (2020): 062422, https://doi.org/10.1103/PhysRevE.101.062422.

26. R. L. Pinals, D. Yang, A. Lui, W. Cao, and M. P. Landry, "Corona Exchange Dynamics on Carbon Nanotubes by Multiplexed Fluorescence Monitoring," *Journal of the American Chemical Society* 142 (2020): 1254–1264, https://doi.org/10.1021/jacs.9b09617.

27. X. Bai, Z. Li, S. Jockusch, N. J. Turro, and J. Ju, "Photocleavage of a 2-nitrobenzyl Linker Bridging a Fluorophore to the 5′ End of DNA," *PNAS* 100 (2003): 409–413, https://doi.org/10.1073/pnas.242729099.

28. M. Zheng, A. Jagota, M. S. Strano, et al., "Structure-Based Carbon Nanotube Sorting by Sequence-Dependent DNA Assembly," *Science* 302 (2003): 1545–1548, https://doi.org/10.1126/science.1091911.

29. J. D. Hirsch, L. Eslamizar, B. J. Filanoski, et al., "Easily Reversible Desthiobiotin Binding to Streptavidin, Avidin, and Other Biotin-binding Proteins: Uses for Protein Labeling, Detection, and Isolation," *Analytical Biochemistry* 308 (2002): 343–357, https://doi.org/10.1016/S0003-2697(02)00201-4.

30. Z. Zhu, R. Yang, M. You, X. Zhang, Y. Wu, and W. Tan, "Single-walled Carbon Nanotube as an Effective Quencher," *Anal Bioanal Chem* 396 (2010): 73–83, https://doi.org/10.1007/s00216-009-3192-z.

31. R. Yang, J. Jin, Y. Chen, et al., "Carbon Nanotube-Quenched Fluorescent Oligonucleotides: Probes That Fluoresce Upon Hybridization," *Journal of the American Chemical Society* 130 (2008): 8351–8358, https://doi.org/10.1021/ja800604z.

32. R. L. Pinals, D. Yang, D. J. Rosenberg, et al., "Quantitative Protein Corona Composition and Dynamics on Carbon Nanotubes in Biological Environments," *Angewandte Chemie (International ed in English)* 59 (2020): 23668–23677, https://doi.org/10.1002/anie.202008175.

33. K. Umemura, S. Sato, G. Bustamante, and J. Y. Ye, "Using a Fluorescence Quenching Method to Detect DNA Adsorption Onto Single-walled Carbon Nanotube Surfaces," *Colloids and Surfaces B, Biointerfaces* 160 (2017): 201–206, https://doi.org/10.1016/j.colsurfb.2017.09.029.

34. S. Nishitani, K. Ao, A. Jalil, et al., "Redox Dye–mediated Fluorescence Energy Transfer of Carbon Nanotube–based Nanosensors," *PNAS* 122 (2025): e2419666122, https://doi.org/10.1073/pnas.2419666122.

35. F. K. Brunecker, F. Schöppler, and T. Hertel, "Interaction of Polymers With Single-Wall Carbon Nanotubes," *J Phys Chem C Nanomater Interfaces* 120 (2016): 10094–10103, https://doi.org/10.1021/acs.jpcc.6b02198.

36. M. S. Dresselhaus, G. Dresselhaus, and R. Saito, "Physics of Carbon Nanotubes," *Carbon N Y* 33 (1995): 883–891, https://doi.org/10.1016/0008-6223(95)00017-8.

37. S. M. Bachilo, L. Balzano, J. E. Herrera, F. Pompeo, D. E. Resasco, and R. B. Weisman, "Narrow (n, m)-Distribution of Single-Walled Carbon Nanotubes Grown Using a Solid Supported Catalyst," *Journal of the American Chemical Society* 125 (2003): 11186–11187, https://doi.org/10.1021/ja036622c.

38. F. Schöppler, C. Mann, T. C. Hain, et al., "Molar Extinction Coefficient of Single-Wall Carbon Nanotubes," *J Phys Chem C Nanomater Interfaces* 115 (2011): 14682–14686, https://doi.org/10.1021/jp205289h.

39. M. M. Safaee, M. Gravely, C. Rocchio, M. Simmeth, and D. Roxbury, "DNA Sequence Mediates Apparent Length Distribution in Single-Walled Carbon Nanotubes," *ACS Appl Mater Interfaces* 11 (2019): 2225–2233, https://doi.org/10.1021/acsami.8b16478.

40. K. R. Hinkle and F. R. Phelan Jr, "Solvation Free Energy of Self-Assembled Complexes: Using Molecular Dynamics to Understand the Separation of ssDNA-Wrapped Single-Walled Carbon Nanotubes," *J Phys Chem C Nanomater Interfaces* 124 (2020): 13127–13140, https://doi.org/10.1021/acs.jpcc.0c00983.

Supporting Information

Additional supporting information can be found online in the Supporting Information section.

Supporting File: The authors have cited additional references within the Supporting Information [36–40].